

Thermal and Hydraulic Analysis of the Adsorption Bed of the Adsorptive Thermal Battery

by

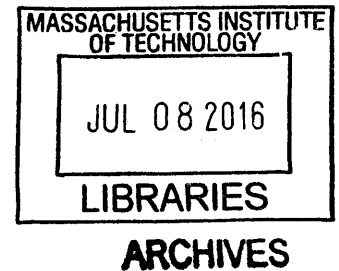
Feyza Haskaraman

Submitted to the
Department of Mechanical Engineering
in Partial Fulfillment of the Requirements for the Degree of
Bachelor of Science in Mechanical Engineering

at the

Massachusetts Institute of Technology

February 2016



©2016 Massachusetts Institute of Technology. All rights reserved.

Signature redacted

Signature of Author: _____

Department of Mechanical Engineering
Jan 15, 2016

Signature redacted

Certified by: _____

Evelyn N. Wang
Associate Professor of Mechanical Engineering
Thesis Supervisor

Signature redacted

Accepted by: _____

Anette Hosoi
Professor of Mechanical Engineering
Undergraduate Officer

Thermal and Hydraulic Analysis of the Adsorption Bed of the Adsorptive Thermal Battery

by

Feyza Haskaraman

Submitted to the Department of Mechanical Engineering
on January 15th, 2016
in Partial Fulfillment of the
Requirements for the Degree of

Bachelor of Science in Mechanical Engineering

ABSTRACT

Electric vehicles (EVs) have a drawback of relatively short drive range that affects their adoption rate. In order to increase the drive range of EVs, replacing heating, ventilation and air conditioning (HVAC) system with a novel absorbent system of materials and methods is widely investigated. This work focuses on the analysis of the design of such a system to suggest efficiency improvements. The thermal insulation and choice of pump required for the optimal function of the adsorptive bed that carries the novel material are analyzed respectively to understand system performance. A thermal resistance analysis was performed in order to understand the undesirable heat loss from the system that decreases the efficiency. Moreover, pressure loss in the piping system was determined theoretically to choose a compatible pump. This analysis also resulted in a modular code that can be used to test different design parameters for future work.

Nomenclature:

Re: Reynolds Number

Pr : Prandtl number

Gr: Grashof number

Nu: Nusselt Number

Ra: Raleigh Number

k: Thermal conductivity (W/m K)

A_{CS}: Area Crosssection (m²)

p_{minor}: Minor Pressure losses (Pa)

p_{major}: Minor Pressure losses (Pa)

T: Temperature (K)

t: thickness (m)

R: Thermal resistance ($\frac{K}{W}$)

ε: Emmisivity

σ = Stefan Boltzman Constant ($\frac{W}{m^2 \times K^4}$)

Thesis Supervisor: Evelyn N. Wang

Title: Associate Professor

Table of Contents

Abstract	2
List of Figures	4
Acknowledgements	5
1. Introduction	6
2. Background	6
2.1 ATB System	6
2.2 Adsorbents	7
2.3 Thermal Adsorptive Bed Design	7
3. Thermal System Analysis	10
3.1 Basic Model: Insulation Conductive Heat Losses	10
3.2. Complex Model: Conduction, Convection, and Radiation	10
3.2.1. Thermal Resistance Analysis: Convection from the Surfaces	11
3.2.2. Thermal Analysis: Radiation Resistance	13
3.2.3. Thermal Analysis: Insulator Conductive Resistance	13
4. Hydraulic System Analysis	14
4.1 Pressure Drop Analysis	16
4.2 Pump Sizing	
5. Summary and Conclusion	17
6. Appendices	18
Appendix A: Thermal Analysis Matlab Code	18
Appendix B: Pressure Drop Analysis Matlab Code	21
7. Bibliography	23

List of Figures

Figure 1:	ATB system modeled in discharge and recharge mode	7
Figure 2:	Current design of the ATB adsorption bed	8
Figure 3:	Conductive heat loss of the insulation/ latest dimensions of adsorption bed	9
Figure 4:	Heat rate loss with respect to thickness and temperature difference	10
Figure 5:	Model of the conduction, convection and radiation heat losses	10
Figure 6:	Heat resistance circuitry of the adsorptive bed	11
Figure 7:	Pressure drop in the pipe and appropriate pump choices	16

Acknowledgements

I would like to thank MIT ATB team for giving me the chance to analyze and work on the Advanced Adsorptive System, especially Dr. Sameer Rao mentoring and coaching me from the start to end of this project. The learning and findings of this thesis would have never happened without his help.

1. Introduction

This work analyzes the current design of Adsorptive Thermal Batteries (ATBs) to verify the design decisions and suggest improvements for higher efficiency. The focus of the work will be the adsorption bed that is one of many parts of the ATB system, including evaporator/condenser/reservoir. At the under-saturated liquid/vapor state, adsorption bed adsorbs vapor, releasing heat and reducing the internal pressure. The reverse of this process can be achieved by adding heat to the adsorption bed to cause the water molecules to go back to the gas state (desorb), free the adsorption bed, and condense back at the condenser and accumulate to be re-pumped [1].

The adsorption bed has MgY (zeolite), which was developed for high performance applications [2] due to its high adsorption capacity and high-energy of adsorption. The ATB system was designed using this material to create an adsorption climate control system for electric vehicles. Just like any other thermal system, heat needs to be transferred to or removed from the adsorption bed to the cabin. During the operation of the adsorption bed, exposure to the environment creates unwanted heat loss from the bed to the environment. These losses become more important during desorption (recharge state) when the system is being returned to its initial configuration by desorbing adsorbate from the adsorption bed. This is because the energy flux from the environment to the adsorption bed will work against the energy input to desorb water molecules. It is, therefore, crucial to understand how much power is lost while recharging the system. Moreover, a pump needs to be carefully selected to match the heating and cooling requirements of ATB.

Section 2 explains the current design of ATB and it will be followed by Section 3 and 4 where the modeling of the system and the equations used for analysis will be discussed. Section 5 will detail the results of the analysis and the future prototype redesign suggestions for higher efficiency.

2. Background

2.1.ATB System

The Advanced Thermo-Adsorptive Battery (ATB) concept is designed to replace the heating, ventilation, and air-conditioning (HVAC) in electric vehicles depending on the season (summer/winter). This system consists of 4 main components – reservoir, evaporator, adsorption bed, and condenser- to create a cyclic system of evaporation and condensation of the adsorbate that can be reversed with an input energy, recharging the system by returning it to its starting configuration [2]. ATB system in two different modes is shown in Figure 1.

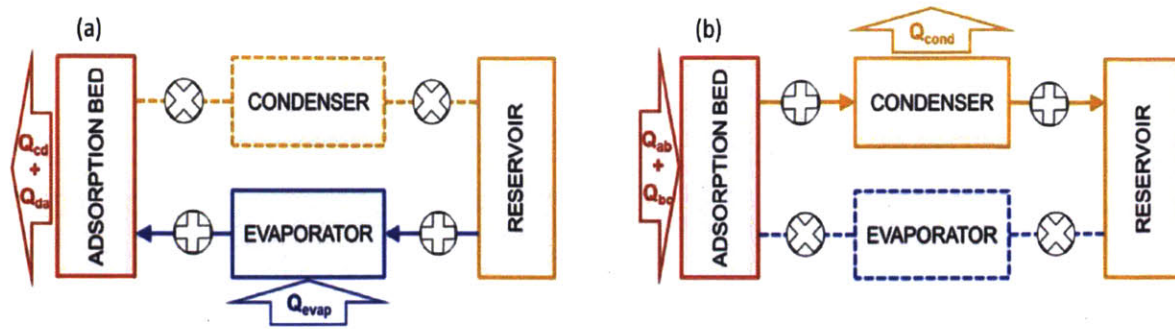


Figure 1: ATB system model in discharge and recharge mode respectively. ATB in discharge mode takes in water from the reservoir, passes it through the evaporator that is then adsorbed by the adsorption bed. In the recharge mode, heat is added to the adsorption bed, by which water vaporizes, condenses to be sent to the reservoir. Image previously appeared in [2].

ATB system's functional operation (cooling& heating) takes place during discharge mode as shown in Figure 1.a. The adsorbate is taken from the reservoir and passed through the evaporator, where the heat is taken from the cabin (20-25°C) in the summer and from the environment (10-15 °C). Even in the winter this exchange can occur because the adsorbate can vaporize at 3 °C via an expansion valve used to pump the adsorbate [4]. At the evaporator, the adsorbate changes phase from liquid to gas, hence cooling the vehicle in the summer. The vapor then passes through the adsorption bed where the adsorbent (zeolite) captures the vapor molecules exothermally that releases the heat of adsorption, which can be used as a heating source in the winter. When the system is in the recharging mode, however, there is an input of heat into the adsorption bed that frees the bed from the adsorbent and increases the pressure. Heating and cooling takes place while cruising, whereas, recharging takes place when the EV is on the grid and its battery is being charged [5].

2.2 Adsorbents

With the advancements in the water-adsorptive materials, the batteries that use heat become more and more appealing for various engineering applications. These batteries emerged as alternates to the currently available batteries. Adsorbents are micro-porous solids that form covalent or Van der Waals bonds with the adsorbate that is in vapor form. Adsorbates bind to various sites on the microstructures of the adsorbate giving out energy as heat. Currently, adsorbent used by the ATB research group is zeolite (MgY), which will form physisorption with water vapor. The material characterizes the heat of adsorption and it is a function of the relative pressure at a given temperature. The heat of adsorption is not constant in time but inversely proportional with the uptake of water. However, because the uptake with respect to time is not of the utmost importance, assuming a constant average heat of adsorption will be practical. This average uptake is as high as 1.7 times the heat of vaporization (h_{fg}) [5].

2.3. Thermal Adsorptive Bed

The current design of the thermal adsorptive bed includes zeolites arranged in a finlike manner to increase the surface exposure of the material to capture more adsorbate. The bed has a piping of a length of 6.4 m, running inside with a diameter of 0.006 mm, carrying solution of ethylene glycol and water. The enclosure is made out of chemically inert stainless steel. There are heaters on the sides of the adsorption bed that are activated during the recharging mode [7].

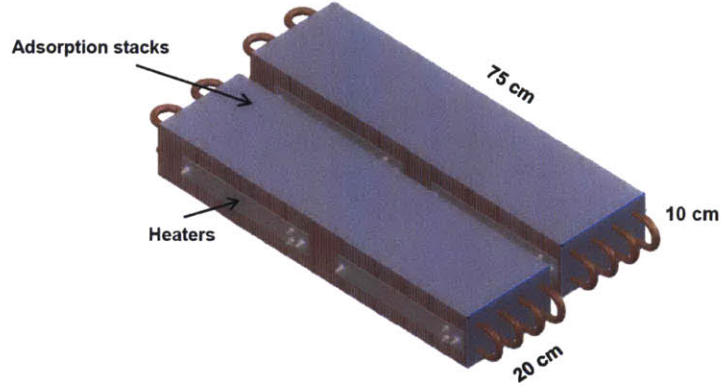


Figure 2: Current overall design of the ATB adsorption bed as appeared in [6]. Latest dimensions are shown in Figure 3. Diameter of 6 mm tube runs inside the zeolite stacks carrying 52% ethylene glycol and 48% water [7].

3. Thermal Analysis of the System

ATB system is not a closed system; it is exposed to the external factors that cause inefficiencies and energy losses. This section analyzes the heat losses from the system using two different models. The first model assumes the losses are only due to the undesired heat loss through the insulator. The second model integrates the heat losses that might occur due to convection and radiation besides conduction. Using thermal modeling and analysis, these problems can be quantified and optimal solutions can be implemented.

3.1. Basic Model: Insulation Conductive Heat Losses

When a hot material is covered with insulation, a material with relatively small conductive coefficient, the aim is to minimize the transfer of energy from the high temperature body to lower temperature body due to the interactions between the particles (conduction). Under steady conditions, where the temperature distribution is linear, heat loss rate and temperature gradient can be quantified with the conductive heat flow equation (1) where k is the conduction coefficient, A_{cs} is the cross sectional area, ΔT is the temperature change and t is the thickness of the material [6].

$$\dot{Q} = -kA_{cs} \frac{\Delta T}{t} \quad (1)$$

To describe thermal systems, an analogy to the electric circuits is useful. Heat loss rate is analogous to the current in the wires and temperature difference (ΔT) to the

voltage drop over a resistance denoted as R. For conduction for example, we can define the resistance as follows:

$$\dot{Q} = \frac{\Delta T}{R_{conductive}} \quad (2)$$

$$R_{conductive} = \frac{t}{kA_{CS}} \quad (3)$$

Using the principles of these two equations, the first analysis was made to see how different thicknesses of insulation material affect the resultant heat loss. For this analysis and the rest, temperature at the adsorptive bed is assumed to be at 250 °C and the outside temperature to be 25 °C. This analysis is also helpful to see if the system can be simplified into a less complex version after comparing it to a more complex second model. The conductive heat coefficient of the insulation material is 0.050 W/mK.

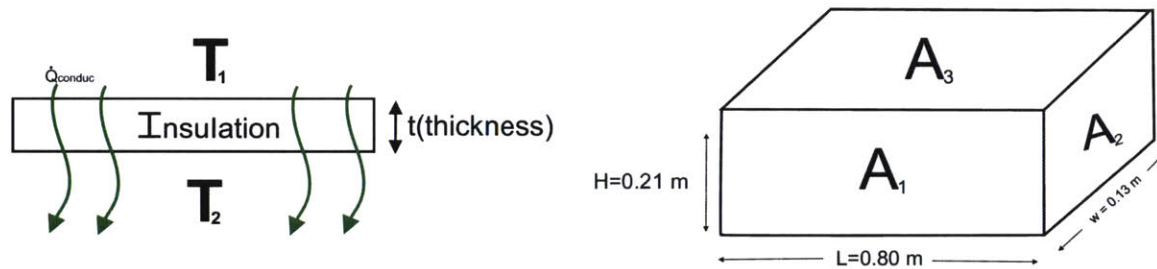


Figure 3: Conductive heat loss from the inner enclosure to the environment modeled (on the left). Latest dimensions of the bed that is used in this analysis, as appeared in [7].

Initial analysis suggests that the insulation k-factor is 1.20 for a thickness of 1 in which was the design choice for this particular iteration. Maximum heat loss due to the temperature change in the range provided is around 100 W. This finding was used to compare this basic modeling to the more complex modeling of the system that will be discussed later.

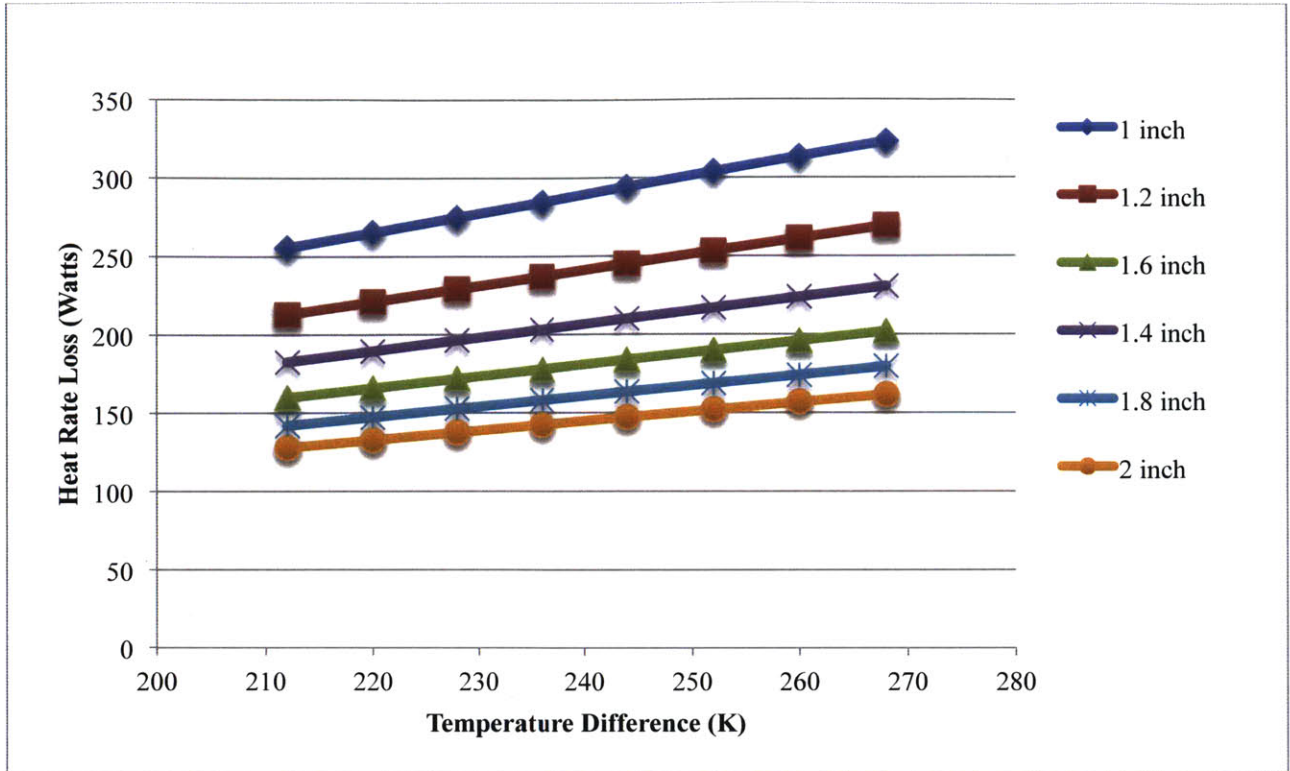


Figure 4: Heat rate loss varies with the thickness and the temperature difference. The design choice for this material was 1 in.

3.2. Complex Model: Conduction, Convection, and Radiation

In addition to the conduction, the effects of the radiation and convection from the surface of the insulator were also taken into account in this second set of analysis.

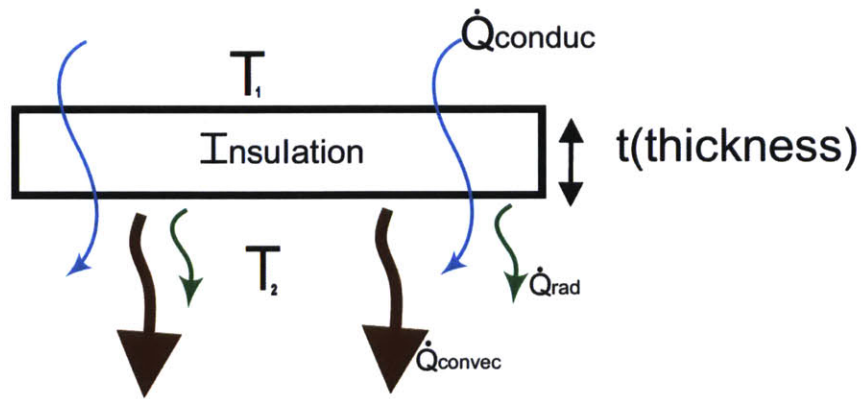


Figure 5: Convective, conductive and radiative heat losses are modeled as a better representation of the system.

Calculations for the analysis were made from the surface of the adsorption bed to the outside environment at T_{air} . Figure 6 below models the resistances around the enclosure. Due to the different orientation of the surfaces with respect to the heat loss direction, the heat loss coefficients at three surfaces were regarded separately.

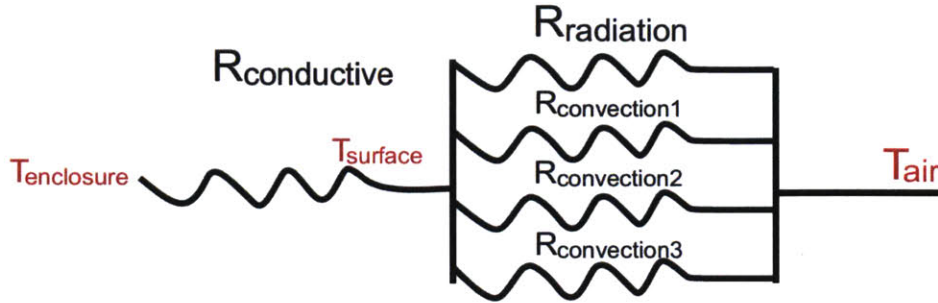


Figure 6: Thermal resistance circuit from the outer face of the enclosure to the air is shown. Heat is conducted by the insulator, which is shown as conductive thermal resistance. From the surface of the insulator, there are convection and radiation from all of the surfaces. Depending on the surface position with respect to the heat flow direction (vertical or horizontal plate), convection coefficient calculations change. Therefore two parallel surfaces are taken as one thermal resistance. There are, therefore, 6 surfaces but only 3 resistances are shown in the figure.

3.2.1. Thermal Resistance Analysis: Convection from the Surfaces

Convection system was divided into three groups, each consisting of two parallel surfaces of the adsorption bed. The vertical and horizontal plates have different convective behaviors, due to the movement of air, that need to be taken into account to find the convective coefficients.

For all of the calculations detailed in this section, all characteristics of air were taken at mean temperature that is found by the equation where T_{bed} is the temperature on the outside of the bed and T_{in} is inside of the bed (4).

$$T_m = \frac{(T_{bed} + T_{in})}{2} \quad (4)$$

For any type of flow, there are two different types of zones characterizing the behavior of the fluid: laminar and turbulent. Two types of forces influence the flow of fluid: shear forces due to the viscosity and inertial forces due to the velocity of the flow. As the molecules are flowing, they tend to stick to the solid surfaces and to each other. This idea is captured in the Newton's law of viscosity where the shear stress is proportional to the velocity gradient. In order to understand which way a fluid will behave in an internal flow, a dimensionless number, Reynolds number (Re), is used.

$$Re = \frac{\rho v d_h}{\mu} \quad (5)$$

where d_h is the hydraulic diameter, v is the flow velocity, μ is the viscosity. Hydraulic diameter is the diameter of the pipe, and $d_h = \frac{4A}{P}$ where A is the cross-sectional area and P is the perimeter. When $Re < 2000$, the flow is characterized as a laminar flow where the molecules

travel at a more organized fashion (velocity profile). When $Re > 4000$, the flow is turbulent and very unstructured.

However, when calculating convective heat coefficient for free convective flow, Reynolds number should be replaced by Grashof number (equation (6)) because buoyancy driven flow usually dominates the inertial flow in forced convective flow. Prandtl number compares the viscous diffusion rate to the thermal diffusion that is inherent to the liquid type and phase (equation (7)), and when combined with Grashof number, Rayleigh number is obtained (equation (9)). Rayleigh number describes whether a fluid is in laminar or turbulent region. While making the calculations for the ATB, the fluid will be assumed to be in the laminar region and this assumption will be tested at the end by looking at the Rayleigh number which will be found using the Grashof number [9].

$$Gr = \frac{gL^3b(T_s - T_{inf})}{\nu^2} \quad (6)$$

$$Pr = \frac{c_p \mu}{k} \quad (7)$$

$$C_{lam} = \frac{0.671}{(1 + (\frac{0.492}{Pr})^{9/16})^{4/9}} \quad (8)$$

$$Ra = Pr \times Gr \quad (9)$$

After finding the Rayleigh number, Nusselt number can be obtained using equation (11), which quantifies the convective to conductive heat transfer. For free convection, an average over the characteristic length, which is perpendicular to the growing boundary layer of flow, is taken where L is the vertical length for the vertical walls and L_{char} is detailed below for the horizontal walls:

$$L_{char} = \frac{A_s}{per} \quad (10)$$

From there, Nusselt number can be used to find average heat convection coefficient that will be described as the \bar{h} with equation (12).

$$Nu = \frac{2}{\log\left(1 + \frac{2}{C_{lam} Ra^{0.25}}\right)} \quad (11)$$

$$\bar{h} = \frac{Nu k_{air}}{L} \quad (12)$$

At the end of the experiment, it can be back solved to see if the assumption of laminar flow is indeed true by looking at the Rayleigh number that is found by the equation (9). The flow is laminar if $Ra_L < 10^9$ which was true for all the Ra values used in the analysis.

Once the convective coefficients are determined, the convection from the surfaces can be found by using the equation below where A is the surface area and \bar{h} is the convective coefficient.

$$R_{convective} = \frac{1}{A\bar{h}} \quad (13)$$

It is important to point out that the Rayleigh number (Ra) to Nusselt number (Nu) relation used above has been shown to be not accurate (equation (11)) for all directions. For a cold plate facing upward and hot plate facing downward, the plate itself acts as an obstruct to the flow of fluid. The flow needs to travel horizontally before it can flow around the plates. For improved accuracy, each parallel plate needs to be treated separately and with colder and warmer conditions. For now, the parallel surfaces are taken to be equivalent whether or not they are facing upwards or downwards.

3.2.2. Thermal Analysis: Radiation Resistance

Energy transfer from atoms and molecules also occur in electromagnetic waves, which is called heat loss due to radiation emitted from the surfaces at temperature T_s . This radiation heat flow resistance can be approximated into equation (14) with the insulation emissivity constant of 0.85.

$$R_{rad} = \frac{1}{(A_s \sigma \epsilon (T_s^2 + T_{inf}^2)(T_s + T_{inf}))} \quad (14)$$

3.2.3. Thermal Analysis: Insulator Conductive Resistance

The calculations for the conductive heat resistance are very similar to section 3.1 where different thicknesses of insulation for the surfaces were taken into account and the resistance was found using equation (2).

Finally, the heat loss over the conductive resistance should be the same as the heat loss rate over the parallel connection of the convective and radiation resistances. Since the expression below is implicit an iterative approach is taken to solve.

$$\frac{T_b - T_s}{R_{conductive}} = \frac{T_s - T_{inf}}{\left(\frac{1}{R_{radiation}} + \frac{2}{R_{convective1}} + \frac{2}{R_{convective2}} + \frac{2}{R_{convective3}} \right)} \quad (15)$$

The code below shows a simple iterative approach that was taken to solve for the surface temperature (T_s). This algorithm updates the T_s with different values according to the difference between the two sides of the equation. At last, heat loss (Q_{loss}) is found after the convergence is achieved.

```

while abs(fl-fv)>0.05
    T_s=T_s+(fl/fv-1);
%% update all of the equations with new T_s
    fv=(T_s-T_inf)/(1/R_rad_exact+2/Rconvect_1+2/Rconvect_2+2/Rconvect_3)^-1;
    fl=(T_b-T_s)/Rconductive;

end

```

In order to test the reliability of the algorithm, the initial prediction (in range) was changed to see its effects on the resultant value. The resultant value did not vary with the initial predictions showing that the algorithm is reliable.

T_s value of 364 K was reached after 347 iterations. This value is between the adsorptive bed temperature of 473 K and 298 K ambient temperature. Total heat loss is found to be 572 W. In comparison to the initial model where the 175 K temperature difference will account 210 W that is less than the half of the convective and radiation heat losses. Therefore, the model cannot be modeled only by the conductive losses. Another finding from this result is that convective and radiation losses account more than half of the losses. Radiation and convective insulation should be carefully chosen and measures such as decreasing the enclosure surface area should be taken into account in future iterations.

4. Pressure Drop Analysis & Pump Sizing

4.1 Pressure Drop Analysis

Another design concern is choosing the right type and size of the pump used for coolant circulation. If a pump cannot provide enough power, the fluid cannot travel inside the bed and the cooling and heating cannot be achieved. The flow inside the pipes is an internal flow and therefore Reynolds number (Re) is used to characterize the type of flow regime. With specified volumetric flow around 6 L/min, Reynolds number for the fluid inside the pipe with 6 mm diameter is 1.6×10^4 and, therefore, the flow is turbulent.

Darcy-Weisbach equation quantifies the pressure drop in a pipe due to the rough surface of the pipes. The equation includes a dimensionless factor that is called Darcy friction factor (f_D) that depends on the Reynolds number.

$$\frac{1}{\sqrt{f_D}} = -2 \log \left(\frac{2.51}{Re \sqrt{f_D}} \right) \quad (16)$$

Assuming a certain volumetric flow rate to remove enough heat from the system, calculations can be made using pressure drop over a rough pipe and Zygot's linearized equation (17).

$$f_0 = \left(-2 \log \left(\frac{2\varepsilon}{(7.54 d_h)} - \frac{5.02}{Re d_h} \log \left(\frac{2\varepsilon}{d_h^{7/54}} + \frac{13}{Re d_h} \right) \right) \right)^{-2} \quad (17)$$

Once the pressure loss due to the roughness of the pipes in turbulent flow is found using Darcy-Weisbach friction factor (f_0) along the length (l) of the pipe, minor losses due to other piping sections such as U-turns are also taken into account. U turns act as inertial obstacle that causes energy loss in the system. Loss coefficient (ϵ) for U-turns for this case is taken to be 1.5 for the threaded U-turn junctions. Combining both losses, final pressure loss value of 119 psi for 5 L/min flow (V) was achieved. This value is important to understand what type of pump can create this pressure drop.

$$P_{\text{major}} = f_0 \frac{l}{d_h} \left(\frac{V^2 \rho}{2} \right) \quad (18)$$

$$P_{\text{minor}} = \epsilon \rho V^2 \quad (19)$$

$$P_{\text{loss}} = P_{\text{major}} + P_{\text{minor}} \quad (20)$$

In order to choose a pump, ATB system's pressure drop and volumetric flow rate need to be correlated. The finding of 5 L/min with 119 psi pressure drop of the system needs to be accommodated by one of the available pipe options. There is a tradeoff between pressure drop and volumetric flow that the pump needs to achieve. Using the same equations and algorithm, and only changing the flow rate, different pressure drop values can be found. Graphing pressure drop vs. flow rate, a characteristic of the ATB system with its limitations can be fully illustrated. This curve was used in choosing a pipe that can accommodate the needs of the system detailed in section 3.2.

It is also important to understand the bulk temperature of the fluid as it exits the adsorption bed for the efficiency calculations of the evaporator/ condenser. The behavior of the heat flow inside and along the pipe needs to be investigated thoroughly and complicated modeling will be needed. Rather than doing this, a set of cases can be investigated and assumptions can be made. First, a constant power assumption is made to find the bulk temperature. ATB system is assumed to dissipate 1.6 kW of power during cooling. However, highest power requirement is during adsorption and heating cycle due to the fact that enthalpy of adsorption is 1.7 times the enthalpy of vaporization. Using this information, where $x=1$, heat flux over the surface area of the pipe and the bulk temperature is found using equation (21) and equation (22).

$$\dot{q} = 1.6 \times 10^3 \times 1.7 / (\pi d_h l) \quad (21)$$

$$T_m = T_{in} + \frac{\pi d_h \dot{q} l}{\dot{m} c_p} \quad (22)$$

Under constant heat dissipation assumption and an inlet temperature of 308 K, mean outlet temperature is found to be 317 K. Secondly, it is also assumed that the surface temperature of the

pipe is constant along the pipe. Equation (23) shows how a constant surface temperature can be predicted. It is assumed that the temperature is linearly increasing from the temperature at the core with a convective heat flux (heat rate as used above).

$$T_s = T_{in} + \frac{\dot{q}}{h} \quad (23)$$

Using constant surface temperature, the mean temperature was found using the equation below to be 309 K. (24)

$$T_m = T_s - (T_s - T_{in})e^{\frac{-\pi d_h \bar{h}}{(\dot{q} \times c_p)}}$$

Comparing these two temperatures, constant heat flux assumption seems to have given a more accurate result around 317 K since 1 K temperature change of the coolant seems very optimistic for ATB system.

4.2 Pump Sizing

Pressure drop analysis gives us information about what type of pump is needed for the system to function according to the requirements. After some market research, several pumps were found and graphed with the pressure drop vs. flow rate. Intersection of the ATB system behavior is generated with the calculations detailed above. The usable two pumps are SHURflo 8000 series diaphragm pumps because the pressure drop curves intersect with ATB system operational curve. If 5059-1311-D011 were used, the volumetric flow where it is functional would exceed the requirements.

The design choice for the rest of the system can be made based on the volumetric flow where the pump curve and the ATB system curve intersect, that is at 3 L/min, 3.2 L/min and 4.2 L/min respectively for the models 543, 343, and 643. Referring back to the initial flow requirement of 5 L/min, best choice of pump is the SHURflo 800-643-236 pump that has volumetric flow around 4.2 L/min.

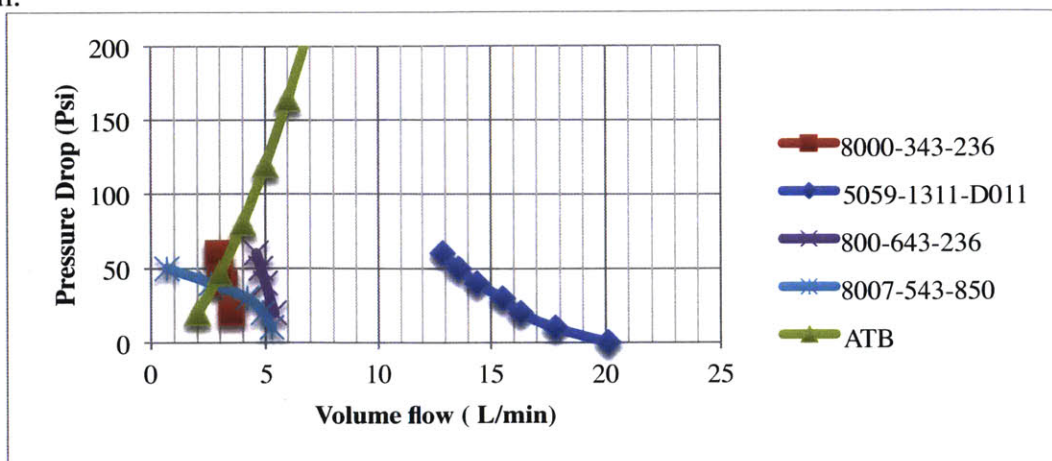


Figure 7: Pressure drop and volume flow relationship of the pumps of the shelf and the ATB system behavior shows that all 8000 series pumps would be compatible but SHURflo 800-643-236 would perform closest to the specs.

5. Summary and Conclusions

This work describes analysis of the ATB system to understand the heat losses from the battery bed during operation, especially during recharge cycle. A final surface temperature of the enclosure was determined along with the losses that can be a factor in the choice of insulations. The second set of analysis was made on the hydraulic system to make design decisions regarding the choice of pump which pumps the coolant that runs inside the adsorption bed to exchange heat with the adsorption bed. An optimal pump option was highlighted which can satisfy the requirements of the system with the volumetric flow and the pressure drop that will be experienced along the pipe. While running this analysis, a highly flexible calculation tool (Appendix A & B) is created for the team to use to test various variables with ATB system design and integration.

Theoretical findings of this analysis were tried to be as close to the real system by considering an exhaustive list of factors. However, the results do not go beyond theoretical calculations. Preliminary data is needed to make design decisions. In future work, the performance of the system needs to be measured by decreasing the surface area of the bed, using the pump recommended in order to ensure that the improvements foreseen can be made with these design changes.

6. Appendices

Appendix A: Thermal Analysis Matlab Code

```
%The temperatures at the start and end of the battery
T_s=400;
T_b=250+273;
T_inf=298;
T_mid=(T_b+T_inf)/2;
g=9.81;

%characteristics of air
b=2.68*10^-3;
v=23.06*10^-6;
k_air=0.0314;

%characteristics of the box
k=0.05;
t_2=0.00508;
t_1=0.00635;

%Areas of the surfaces
A_s_1=0.80*0.21; %surface 1
A_s_2=0.13*0.21;%surface 2
A_s_3=0.80*0.13; %surface 3
per=(0.80+0.13*2); %surface 3 perimeter
A_s=2*(A_s_1+A_s_2+A_s_3);

%Radiation variables and equations
sigma=0.85;
epsilon=5.6703*10^-8;

R_rad_exact=1/(A_s*sigma*epsilon*(T_s^2+ T_inf^2)*( T_s+T_inf));

fv=(T_s-T_inf)/(1/R_rad_exact+2/Rconvect_1+2/Rconvect_2+2/Rconvect_3)^-1;
fl=(T_b-T_s)/Rconductive;
i=0;
```

```

%length of the vertical surfaces
L_1=0.21;
L_2=0.21;

%length of the horizontal surfaces
L_char=A_s_3/(per);

%Finding convective coefficients for the first vertical surface
Pr_1=0.71; % for T_mid from the excel graph
Gr_1=g*L_1^3*b*(T_s-T_inf)/(v^2);
Ra_1=Pr_1*Gr_1;
C_lam=0.671/(1+(0.492/Pr_1)^9/16)^(4/9);
Nu_1=2/log(1+2/(C_lam*Ra_1^0.25));
h_bar_1=Nu_1*k_air/L_1;%vertical plane

%Finding convective coefficients for the second vertical plane
Pr_2=0.71; % for T_mid from the excel graph
Gr_2=g*L_2^3*b*(T_s-T_inf)/(v^2);
Ra_2=Pr_2*Gr_2;
C_lam_2=0.671/(1+(0.492/Pr_2)^9/16)^(4/9);
Nu_2=2/log(1+2/(C_lam_2*Ra_2^0.25));
h_bar_2=Nu_2*k_air/L_2;%vertical plane

%Finding convective coefficients for the second horizontal plane
Pr_3=0.71; % for T_mid from the excel graph
Gr_3=g*L_char^3*b*(T_s-T_inf)/(v^2);
Ra_3=Pr_3*Gr_3;
C_lam_3=0.671/(1+(0.492/Pr_3)^9/16)^(4/9);
Nu_3=2/log(1+2/(C_lam_3*Ra_3^0.25));
h_bar_3=Nu_3*k_air/L_char;%vertical plane

Rconductive_1= t_1/(k*A_s_1);
Rconductive_2=t_2/(k*A_s_2);
Rconductive_3=t_2/(k*A_s_3);
Rconductive=(2/Rconductive_1+2/Rconductive_2+2/Rconductive_3)^-1;

Rconvect_1=1/(h_bar_1*A_s_1);
Rconvect_2=1/(h_bar_2*A_s_2);
Rconvect_3=1/(h_bar_3*A_s_3);
R_rad_exact=1/(A_s*sigma*epsilon*(T_s^2+ T_inf^2)*( T_s+T_inf));

```

```

%iteration for convergence
while abs(fl-fv)>0.05
    T_s=T_s+(fl/fv-1);

    %%%
    %Finding convective coefficients for the first vertical surface
    Pr_1=0.71; % for T_mid from the excel graph
    Gr_1=g*L_1^3*b*(T_s-T_inf)/(v^2);
    Ra_1=Pr_1*Gr_1;
    C_lam=0.671/(1+(0.492/Pr_1)^9/16)^(4/9);
    Nu_1=2/log(1+2/(C_lam*Ra_1^0.25));
    h_bar_1=Nu_1*k_air/L_1;%vertical plane

    %Finding convective coefficients for the second vertical plane
    Pr_2=0.71; % for T_mid from the excel graph
    Gr_2=g*L_2^3*b*(T_s-T_inf)/(v^2);
    Ra_2=Pr_2*Gr_2;
    C_lam_2=0.671/(1+(0.492/Pr_2)^9/16)^(4/9);
    Nu_2=2/log(1+2/(C_lam_2*Ra_2^0.25));
    h_bar_2=Nu_2*k_air/L_2;%vertical plane

```

Appendix B: Pressure Drop Analysis Matlab Code

```
%Pipe Specs
l = 6.4;%length of duct or pipe
dh=0.006; %hydraulic diameter (6mm)
A=dh*2*pi*l;
flowthru=7; %in L/min
v= (flowthru*0.001/60)/ (0.006^2*pi/4); %0.0000833/; % flow velocity 0.736 m/s
%Vvol=5*10^-3/60; %volumetric flow rate (m/s)
g=9.81; % acceleration
uTurns=7;
%Fluid 52% Ethylene glycol and 48% water
epsilon=1.5; %minor loss coefficient 0.2 for flanged, 1.5 for threaded
rho40C=1074.6; %kg/m^3
mu=1.78*10^-3; % viscosity in PaSec
vis=mu/rho40C; %dynamicviscosity
Re=rho40C*v*dh/mu;
eps_pipe=0.015*0.001;
f0=(-2*log10(2*eps_pipe/(7.54*dh)-5.02/(Re*dh)*log10(2*eps_pipe/(7.54*dh)+13/(Re*dh))))^-2;
p_minor = epsilon*rho40C*v^2;
%p_minor=50*dh*9.81*rho40C;
p_major = f0*(l/dh)*(v^2*rho40C/2); % Darcy-weisbach equation
p_loss=p_major+p_minor*7;
p_loss_psi=p_loss*0.000145038;
```

```

%Liquid properties/Pr= c_p* mu/k;
Pr=16.913;
T_in= 35+273;
k=0.44169; %(W/(m*K))
n= 0.33; % for heating, 0.33 for cooling
c_p=3329;

%Nu_1= 0.23* Re^0.8*Pr^n;Re>100000
% Finding the Nusselt Number
f=(0.79*log(Re)-1.64)^-2; % Darcy Friction factor
Nu_2= (f/8*(Re-1000)*Pr)/(1+12.7* (f/8)^0.5*(Pr^(2/3)-1));

% Finding the heat convective coefficient
h_bar=Nu_2*k/dh;

%Constant heat flux
heat_flux=1.6*10^3*1.7/(pi*dh*l);
x=l;
T_m= T_in+ (pi*dh*heat_flux/(mass_flow*c_p)*x);
%prescribed wall temperature

%Isothermal
T_s=T_in+heat_flux/(h_bar); %Tin/2+
T_m_2= T_s-(T_s-T_in)* exp(-pi*dh*l*h_bar/(mass_flow*c_p));

```

7. Bibliography

- [1] S.Narayanan X. Li, S. Yang, H. Kim, A. Umans, I.S. McKay, E.N. Wang: *Thermal Battery for Portable Climate Control. Applied Energy* 149,104-116,2015
- [2] P.Domanski, *Theoretical Evaluation of the Vapor Compression Cycle with Liquis-Line/Suction-Line Heat Exchanger, Economizer, and Ejector*, NISTIR Report to the U.S. Department of Commerce (1995)
- [3] X. Li, S. Narayanan, V.K. Michaelis, T.Ong, E.G. Keeler, H. Kim, I.S. McKay, R.G. Griffin, E.N. Wang,: *Zeolite Y Absorbents with High Vapor Uptake capacity and Robust Cycling Stability for Potential Applications in Advanced Adsorption Heat Pumps*. *Microporous and Mesoporous Materials* 201, 151-159,2015.
- [4] Huyanho Kim: *Experimental Characterization of Adsorption and Transport Properties for Advanced Thermo-Adsorptive Batteries*.S.M Thesis, University of Illinois at Urbana-Champaign Department of Mechanical Engineering, 2011
- [5] A. Umans : *Small-Scale Advanced-Thermo-Adsorptive Battery Prototype*. S.M Thesis, MIT Department of Mechanical Engineering, 2013
- [6] F. P. Incropera, "Internal Flow," in *Fundamentals of heat and mass transfer*, 6th ed., Hoboken, NJ: John Wiley, 2007, pp. 490–511.
- [7] S. R. Rao, H. Kim, and A. Umans, "ATB Prototype: System Integration and Adsorption Bed Fabrication," in *Program Review*, 2015.